Impact of misfit dislocations on the polarization instability of epitaxial nanostructured ferroelectric perovskites

MING-WEN CHU*[1], IZABELA SZAFRANIAK[1,2], ROLAND SCHOLZ[1], CATALIN HARNAGEA[1,3], DIETRICH HESSE[1], MARIN ALEXE[1] AND ULRICH GÖSELE[1]

[1]Max-Planck-Institut für Mikrostrukturphysik, Weinberg 2, D-06120 Halle (Saale), Germany
[2]Present address: Institute of Materials Science and Engineering, Poznan University of Technology, M. Sklodowska Curie 5 Sq., 60-965 Poznan, Poland
[3]Present address: INRS — Énergie, Matériaux et Télécommunications, 1650 Lionel-Boulet, Varennes, Québec J3X 1S2, Canada
*e-mail: cmingwen@mpi-halle.mpg.de

Published online: 18 January 2004; doi:10.1038/nmat1057

Defects exist in almost all materials[1] and defect engineering at the atomic level is part of modern semiconductor technology[2,3]. Defects and their long-range strain fields can have a negative impact on the host materials[4,5]. In materials with confined dimensions, the influence of defects can be even more pronounced due to the enhanced relative volume of the 'defective' regions. Here we report the dislocation-induced polarization instability of (001)-oriented $Pb(Zr_{0.52}Ti_{0.48})O_3$ (PZT) nanoislands, with an average height of ~9 nm, grown on compressive perovskite substrates. Using quantitative high-resolution electron microscopy[4], we visualize the strain fields of edge-type misfit dislocations, extending predominantly into a PZT region with a height of ~4 nm and width of ~8 nm. The lattice within this region deviates from the regular crystal structure. Piezoresponse force microscopy indicates that such PZT nanoislands do not show ferroelectricity. Our results suggest that misfit engineering is indispensable for obtaining nanostructured ferroelectrics with stable polarization.

The polarization instability of thin ferroelectrics (that is, ferroelectricity vanishing below a critical thickness) has remained an open question for several decades[6,7]. This size-effect issue currently receives considerable experimental[8–11] and theoretical[12–17] attention due to the potential integration of nanoscale ferroelectrics into non-volatile semiconductor memories[9–11]. Considering the electrode/ferroelectrics/electrode geometry used in electrical characterization, the origin of polarization instability in ultrathin simple ferroelectric perovskites[11–17] can be categorized into extrinsic and intrinsic[11]. Two extrinsic origins claimed in the literature are the depolarization field resulting from the incomplete screening of the dipole charges by the electrodes, and the strain imposed by the thick substrate or electrode[11–16]. The effects of relaxation of the free surface of ferroelectrics are rather regarded as of intrinsic origin[11–14,17].

Experimental reports on the critical dimension of simple ferroelectric perovskites[9–11] may be su mmarized as follows: an ultimate thickness of ~4 nm was determined for tetragonal (001)-epitaxial $Pb(Zr_{1-x}Ti_x)O_3$ ($x \geq 0.48$) films[9,11] and randomly oriented $PbTiO_3$ islands[10]. Although the origin of the polarization instability was not clearly addressed therein[9–11], it was pointed out that the ferroelectric size effect should be three-dimensional in nature[10,11]. Theoretical studies of single-crystalline and single-domain (001)-oriented tetragonal perovskites[12–16] indicate that ferroelectrics can be either free from size effects at a thickness of several unit cells, in consideration of only the elastic accommodation of biaxial in-plane compressive strain and/or

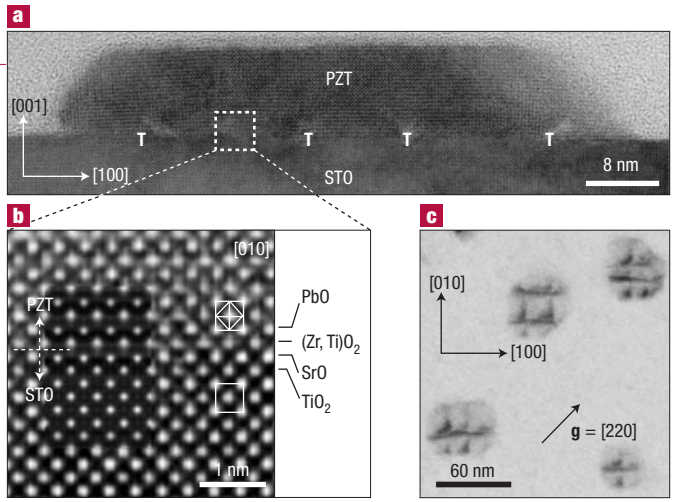

Figure 1 Cross-sectional and plan-view micrographs and calculated contrasts of the PZT nanoislands. a, Cross-sectional HREM image of a (001)-oriented PZT nanoisland in [010] projection; misfit dislocations indicated by **T**. **b**, An enlarged interface zone of **a**; the inserted small white rectangle and square indicate respective PZT and STO lattices; inset (dark area on the left), multislice contrast simulation at $t = 4$ nm and $\Delta f = -60$ nm with $PbO\text{-}(Zr,Ti)O_2\text{-}SrO\text{-}TiO_2$ stacking across the interface. At this imaging condition, bright and dark contrasts represent the cation and anion columns, respectively. **c**, Bright-field plan-view image recorded under **g** = [220] on specimens annealed at 950 °C for 1 h, the dark contrasts showing the network of misfit dislocations.

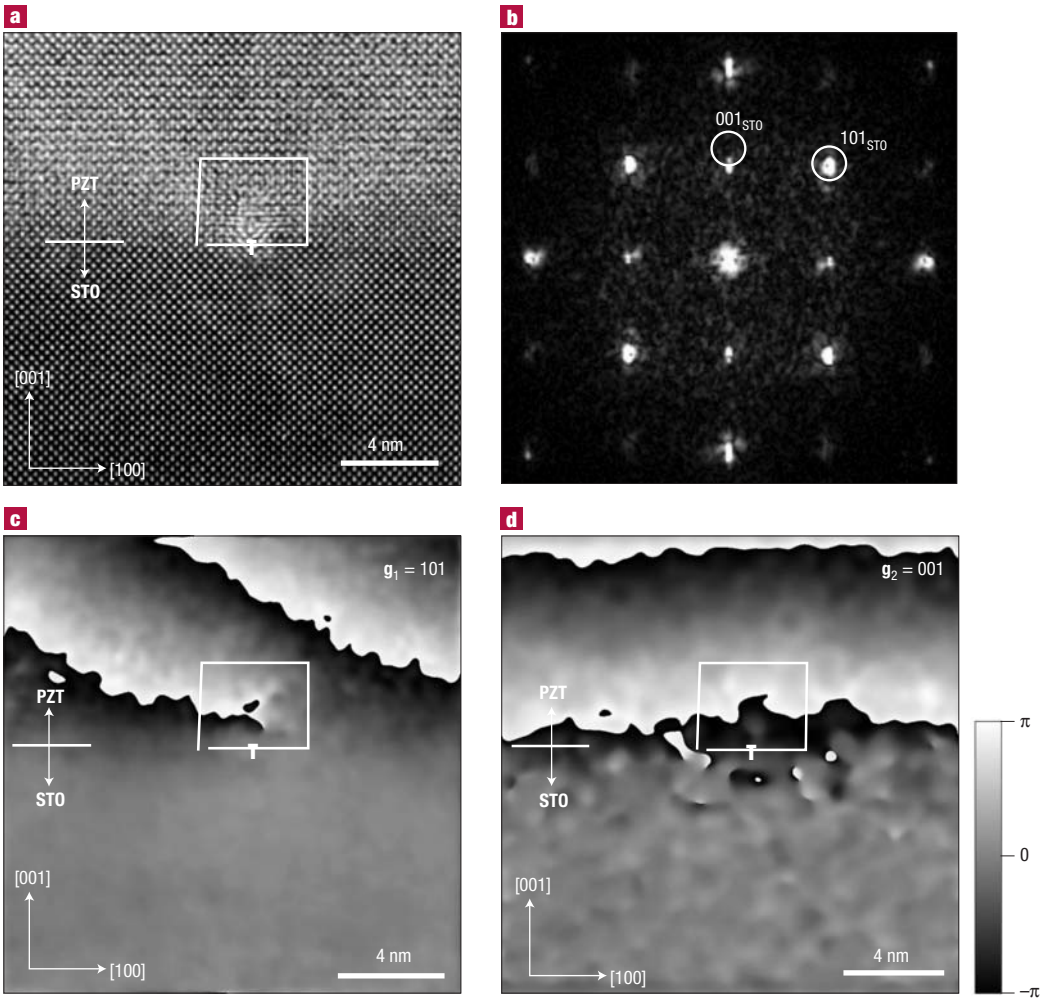

Figure 2 Geometric phase analysis of a misfit dislocation in a PZT nanoisland. **a**, Cross-sectional HREM image of a (001)-epitaxial PZT nanoisland in [010] projection revealing contrasts around the dislocation core and the Burgers circuit indicating $\boldsymbol{b} = a\langle 100\rangle$. **b**, Fourier transform of **a**; (101) and (001) Bragg reflections of STO being used for calculating the respective geometric phase images **c** and **d**. The scale bar on the right shows a normalized phase variation from $-\pi$ to π.

the surface effects[12–15], or exhibiting a polarization instability below the ultimate limit of six unit cells (~2.4 nm, $BaTiO_3$), taking into account both the elastic accommodation of biaxial in-plane compressive strain and the depolarization field[16]. The above divergence in the theoretical predictions[12–16] arises from the different electrical and mechanical boundary conditions considered in the computations[16], for example, screening length of the electrodes, strain conditions, and degree of surface relaxation. The disagreement between experimental results[9–11] and theoretical predictions[12–15] can be associated with the simplification of the electromechanical boundary conditions[12–16] involved in calculations by neglecting defects frequently formed at the interfaces[18,19]. To bridge these experimental[9–11] and theoretical[12–16] gaps it is essential to probe the role of interfacial defects in nanoscale ferroelectrics with a tetragonal perovskite structure.

We performed a high-resolution electron microscopy (HREM) study on epitaxial $Pb(Zr_{0.52}Ti_{0.48})O_3$ (PZT) nanoislands prepared at 800 °C on cubic Nb-doped $SrTiO_3(001)$ substrates (STO) that serve also as bottom electrodes. Details on the growth of the nanoislands by chemical solution deposition (CSD) were reported separately[20]; advanced knowledge in CSD preparation of nanostructured ferroelectrics can be found in ref. 21. The specimens for HREM investigations were prepared by mechanical polishing, dimpling, and then ion milling in a Gatan PIPS system at 3 kV. HREM images were taken on a JEOL 4010 operating at 400 kV with a point resolution of 1.6 Å. Piezoresponse force microscopy (PFM, Autoprobe CP Research, Veeco) measurements of polarizations of the bare nanoislands were performed.

Figure 1a shows a representative cross-sectional HREM image of a PZT nanoisland in the [010] zone axis, revealing the truncated-pyramid morphology with {111} and {110} facets[20] and an average height of ~9 nm and base length of ~50 nm. A careful examination of the experimental contrast of PZT indicates its tetragonality (Fig. 1b). This conclusion was confirmed by multislice image calculations taking into account the [010] orientation and the interfacial stacking[22] of PbO-$(Zr,Ti)O_2$-SrO-TiO_2. From the good agreement between the simulated and experimental contrasts (Fig. 1b), the tetragonal structure of the nanoislands, their epitaxial orientation relationship $(001)_{PZT}[100]_{PZT}\|(001)_{STO}[100]_{STO}$, and an atomically sharp interface were deduced. Most importantly, PZT appears as single-crystalline and single-*c*-domain, that is, the crystallographic *c*-axis is entirely perpendicular to the interface plane. In the absence of the top electrodes, the stabilization of single-*c*-domain nanoislands (that is, absence of

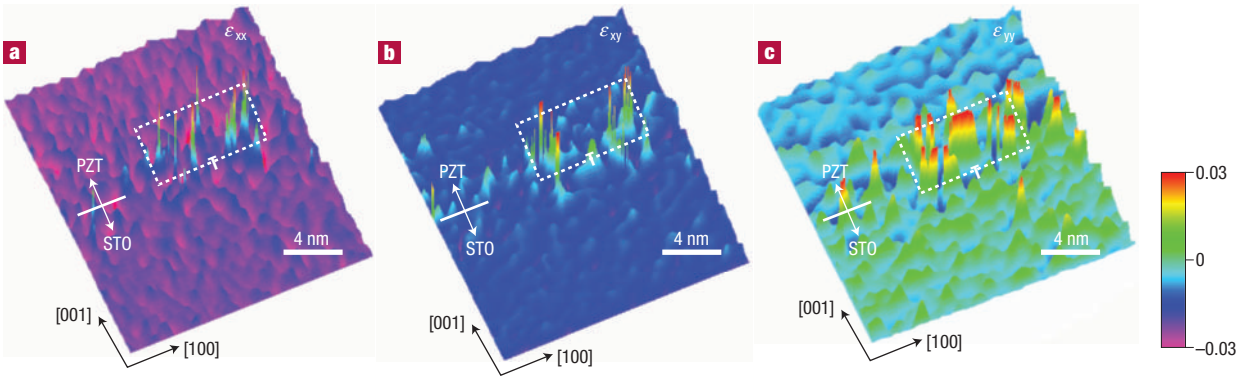

Figure 3 Quantitative measurements of long-range strain fields of the misfit dislocations along [100] and [001] axes using geometric phase analysis. a, In-plane (ε_{xx}), **b**, shear (ε_{xy}), and **c**, out-of-plane (ε_{yy}) strain fields imposed by the misfit dislocations. **T** shows the location of the end-on dislocation line. The dashed rectangles indicate the strain fields of the dislocation core, extending predominantly into the PZT region with an estimated height of ~4 nm and width of ~8 nm.

180° domains) strongly suggests that the imperfectly screened depolarization field[16] plays a negligible role in the polarization instability of these structures. This can, most probably, be ascribed to the non-zero conductivity[11,14,15] or the homogeneous compensation for dipole charges by possible intrinsic surface conducting layers[9,23].

The misfit dislocations at the interface were also visualized in bright-field plan-view transmission electron micrographs (TEMs) (Fig. 1c) recorded under two-beam conditions with $\mathbf{g} = [220]$, where $\mathbf{g}$ is the diffracting reciprocal lattice vector. The dark line contrasts in Fig. 1c represent the orthogonal network of misfit dislocations, and the nanoislands show a rounded square base. The nominal misfit $\boldsymbol{\delta}$ is ~3.4% taking $a_{STO} = 3.905$ Å, $a_{PZT} = 4.036$ Å, and $c_{PZT} = 4.146$ Å into account[24]. The Burgers circuit (Fig. 2a) indicates that the misfit dislocations are of edge type with Burgers vectors $\boldsymbol{b} = a\langle 100\rangle$, the extra half-plane residing on the STO side. Evaluation of the dislocation spacing over tens of nanoislands gives an average of ~13 nm in good agreement with the theoretical value[22] ($\boldsymbol{b}/\boldsymbol{\delta}$ for a relaxed mismatched system) of ~12 nm. This close agreement indicates that the internal strain resulting from the misfit and the spontaneous lattice deformation due to the improper ferroelectric–ferroelastic transition is fully released by misfit dislocations. Taking into account the anisotropic elastic constants of PZT[25] and STO[22], the critical thickness h_c for misfit dislocation formation was calculated within the anisotropic elastic theory[22,26] as $h_c \sim 1.3$ nm. This low value suggests that the misfit dislocations emerge in the early nucleation and growth stage of the paraelectric phase.

In the core region of the misfit dislocation (Fig. 2a), experimental contrasts of PZT are strongly modified by the associated strain fields[27]. To further investigate long-range strain fields within the dislocation core, we performed a geometric phase analysis[4,28] (part of Digital Micrograph 2.5 package, Gatan) on the displacements of atomic columns in Fig. 2a, digitized at an image density of 0.041 nm per pixel.

Taking STO as the reference lattice, its two local $\mathbf{g}$ vectors with the best signal-to-noise ratio (Fig. 2b), $\mathbf{g}_1 = [101]$ and $\mathbf{g}_2 = [001]$, were used to calculate the geometric phase images (Fig. 2c,d) exploiting gaussian masks[4,28], and the corresponding resolution is estimated to be within 1 nm. On the PZT side of Fig. 2c,d, the observed phase gradient with a period of 2π, that is, a lattice periodicity of STO, indicates a difference in spatial frequency across the interface. In Fig. 2d, the apparent geometric phase fluctuation of STO, arising from the slight sample misorientation, thickness variation, and image noise, leads to locally non-zero phase components of STO, subsequently adding certain errors to the geometric phase of PZT.

The geometric phase obtained is related to a corresponding two-dimensional displacement field $u(\mathbf{r})$ by the following formula[4,28], $u(\mathbf{r}) = -(1/2\pi)[P_{g1}(\mathbf{r})\mathbf{a}_1 + P_{g2}(\mathbf{r})\mathbf{a}_2]$ where $\mathbf{r}$ is a position in the image, $P_{g1}(\mathbf{r})$ and $P_{g2}(\mathbf{r})$ are the two geometric phase images (Fig. 2c,d respectively), and $\mathbf{a}_1$ and $\mathbf{a}_2$ are the associated lattice vectors of $\mathbf{g}_1$ and $\mathbf{g}_2$ in real space ($[100]$ and $[\bar{1}01]$, respectively). The x and y components of the two-dimensional displacement field, $u_x(\mathbf{r})$ and $u_y(\mathbf{r})$, can thus be determined by further referring the respective x and y axes to $[100]$ and $[001]$. Moreover, the local distortion of the PZT lattice with respect to STO, e, is given by the gradient of the displacement field ($e_{xx} = \partial u_x(\mathbf{r})/\partial x$, $e_{xy} = \partial u_x(\mathbf{r})/\partial y$, $e_{yx} = \partial u_y(\mathbf{r})/\partial x$, and $e_{yy} = \partial u_y(\mathbf{r})/\partial y$), and the symmetric term of the gradient indicates the strain matrix (ε)[28]. We can thus derive the symmetric, biaxial strain fields ε_{xx} (in-plane), ε_{xy} (= ε_{yx}, shear), and ε_{yy} (out-of-plane), as shown in Fig. 3a–c, respectively, with a resolution comparable to that of the geometric phase images. The non-equivalent colour scale of STO (Fig. 3a–c) is relevant to the phase fluctuation observed in Fig. 2d and the different partial derivative performed. The low average of PZT with respect to STO (Fig. 3c) arises from errors in the corresponding $u_y(\mathbf{r})$ image that is the direct contrast inversion of Fig. 2d. Furthermore, the contribution of the geometric phase noise—related to loss in image contrast within the dislocation core—to the obvious peaks around the dislocation (Fig. 3a–c), though minor, should not be neglected. Note that Fig. 3a–c does not represent the real strain (PZT deformation with respect to the unconstrained lattice) but the deformation of PZT with respect to the STO lattice. However, the measured ε_{xx}, ε_{xy} and ε_{yy} (~ –0.025, ~0.005 and 0, respectively), obtained by comparing the nominal and averaged PZT lattices, indicate that Fig. 3a–c gives reasonable estimations of the actual strain.

In Fig. 3a–c, the associated strain fields of the misfit dislocation are localized on the PZT side because PZT is softer than STO[25]. The strain fields of the dislocation core, triaxial in nature, exhibit a tensile-strained region embedded in a compressive matrix, extending predominantly into PZT and being confined within a region with a height of ~4 nm and a width of ~8 nm.

The partial volume V_p of the truncated pyramids involving eight edge dislocations (Fig. 1a), which is affected by the triaxial strain fields, can be estimated as $V_p \sim 0.57 \pm 0.05$. As ferroelectricity is a cooperative phenomenon of a sufficient number of regular non-centrosymmetric unit cells[11], this significant ratio points to a potential long-range influence on the ferroelectric properties of the PZT nanoislands. On probing polarizations of a large number of bare nanoislands by PFM, we observed that the nanoislands with $V_p \sim 0.6$, that is, an island

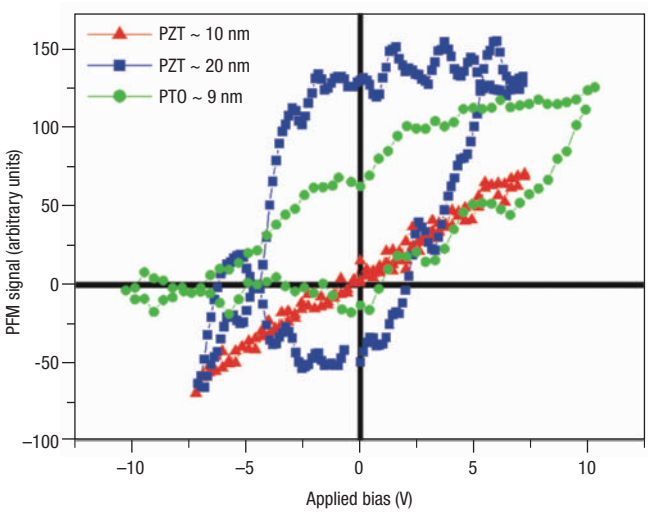

Figure 4 Local piezoelectric hysteresis loops measured by PFM. The linear piezoresponse (red) was measured on individual PZT nanoislands with a height of ~10 nm, whereas those with a height of ~20 nm show well-defined hysteresis loops (blue). The green hysteresis loop was acquired from a single-crystalline and single-*c*-domain PTO nanoisland (~9 nm in height) free from misfit dislocations at the interface.

height of ~10 nm, show an apparent polarization instability (Fig. 4) that should be associated with the distorted PZT lattice within the triaxial strain fields. The PZT lattice deviates from the regular tetragonal structure, and the long-range correlations of local polarizations may thus break down, leading to the polarization instability. By contrast, PZT with an island height of ~20 nm, that is, $V_p \sim 0.3$, shows a well-defined piezoresponse loop (Fig. 4). This triaxial strain scenario further suggests that $Pb(Zr_{1-x}Ti_x)O_3$-type nanoislands with a height of ~9 nm can exhibit long-range polarizations, if the formation of misfit dislocations is avoided. The piezoresponse loop (Fig. 4) recorded from a tetragonal (001)-epitaxial $PbTiO_3$ (PTO) nanoisland grown on STO ($a_{PTO} = 3.895$ Å, $c_{PTO} = 4.142$ Å, and $h_c = 57$ nm, ref. 22), ~9 nm in height and certainly free from misfit dislocations, strongly supports this triaxial strain scenario.

We can thus conclude that misfit strain is a possible extrinsic origin for the polarization instability[11] either (i) in the plastic accommodation regime by misfit dislocations or (ii) in the elastic accommodation regime with a significant biaxial in-plane tensile strain imposed on simple ferroelectric perovskites with an out-of-plane polar axis. By contrast, the elastic accommodation of the in-plane compressive strain could lead to an enhancement of the spontaneous polarization of simple ferroelectric perovskites along the out-of-plane direction[14,15]. In the absence of the depolarization field and with a low intrinsic contribution of the surface relaxation, we thus suggest that elastically, compressively strained epitaxial simple ferroelectric perovskites with an out-of-plane polar axis should be free from polarization instabilities, in excellent agreement with experimental results[9] according to which (001)-epitaxial $Pb(Zr_{0.2}Ti_{0.8})O_3$/STO ($a = 3.931$ Å, $c = 4.133$ Å, and $h_c = \sim 10$ nm; refs 22 and 25) as well as[11,29] $SrRuO_3$/PZT/$SrRuO_3$ ($SrRuO_3$, pseudo-cubic, $a = \sim 3.923$ Å) ultrathin films below 4 nm still show weak ferroelectricity.

Received 15 September 2003; accepted 10 December 2003; published 18 January 2004.

References

1. Stoneham, A. M. *Theory of Defects in Solids* (Clarendon, Oxford, 1985).
2. Ebert, Ph. *et al.* Thermal formation of Zn-dopant-vacancy defect complexes on InP(110) surfaces. *Phys. Rev. B* **53,** 4580–4590 (1996).
3. Estreicher, S. K. Defect theory: Elusive state-of-the-art. *Mater. Today* **6,** 26–35 (2003).
4. Hÿtch, M. J., Putaux, J.-L. & Pénisson, J.-M. Measurement of the displacement field of dislocations to 0.03Å by electron microscopy. *Nature* **423,** 270–273 (2003).
5. Neumark, G. F. New model for interface charge-carrier mobility: The role of misfit dislocations. *Phys. Rev. Lett.* **21,** 1252–1256 (1968).
6. Wurfel, P., Batra, I. P. & Jacobs, J. T. Polarization instability in thin ferroelectric films. *Phys. Rev. Lett.* **30,** 1218–1221 (1973).
7. Batra, I. P., Wurfel, P. & Silverman, B. D. Phase transition, stability, and depolarization field in ferroelectric thin films. *Phys. Rev. B* **8,** 3257–3265 (1973).
8. Bune, A. V. *et al.* Two-dimensional ferroelectric films. *Nature* **391,** 874–877 (1998).
9. Tybell, T., Ahn, C. H. & Triscone, J.-M. Ferroelectricity in thin perovskite films. *Appl. Phys. Lett.* **75,** 856–858 (1999).
10. Roelofs, A., Schneller, T., Szot, K. & Waser, R. Piezoresponse force microscopy of lead titanate nanograins possibly reaching the limit of ferroelectricity. *Appl. Phys. Lett.* **81,** 5231–5233 (2002).
11. Kohlstedt, H., Pertsev, N. A. & Waser, R. Size effects on polarization in epitaxial ferroelectric films and the concept of ferroelectric tunnel junctions including first results. *Mat. Res. Soc. Symp. Proc.* **688,** 161–172 (2002).
12. Ghosez, Ph. & Rabe, K. M. Microscopic model of ferroelectricity in stress-free $PbTiO_3$ ultrathin films. *Appl. Phys. Lett.* **76,** 2767–2769 (2000).
13. Meyer, B. & Vanderbilt, D. *Ab initio* study of $BaTiO_3$ and $PbTiO_3$ surfaces in external electric fields. *Phys. Rev. B* **63,** 205426 (2001).
14. Zembilgotov, A. G., Pertsev, N. A., Kohlstedt, H. & Waser, R. Ultrathin epitaxial ferroelectric films grown on compressive substrates: Competition between the surface and strain effects. *J. Appl. Phys.* **91,** 2247–2254 (2002).
15. Pertsev, N. A., Kukhar, V. G., Kohlstedt, H. & Waser, R. Phase diagrams and physical properties of single-domain epitaxial $Pb(Zr_{1-x}Ti_x)O_3$ thin films. *Phys. Rev. B* **67,** 054107 (2003).
16. Junquera, J. & Ghosez, Ph. Critical thickness for ferroelectricity in perovskite ultrathin films. *Nature* **422,** 506–509 (2003).
17. Li, S. *et al.* Size effects in nanostructured ferroelectrics. *Phys. Lett. A* **212,** 341–346 (1996).
18. Pöykkö, S. & Chadi, D. J. Dipolar defect model for fatigue in ferroelectric perovskites. *Phys. Rev. Lett.* **83,** 1231–1234 (1999).
19. Chu, M.-W., Ganne, M., Caldes, M. T., Gautier, E. & Brohan, L. X-ray photoemission spectroscopy characterization of the electrode-ferroelectric interfaces in Pt/$Bi_4Ti_3O_{12}$/Pt and Pt/$Bi_{3.25}La_{0.75}Ti_3O_{12}$/Pt capacitors: Possible influence of defect structure on fatigue properties. *Phys. Rev. B* **68,** 014102 (2003).
20. Szafraniak, I., Harnagea, C., Scholz, R., Hesse, D. & Alexe, M. Ferroelectric epitaxial nanocrystals obtained by a self-patterning method. *Appl. Phys. Lett.* **83,** 2211–2213 (2003).
21. Waser, R., Schneller, T., Hoffmann-Eifert, S. & Ehrhart, P. Advanced chemical deposition techniques – from research to production. *Integ. Ferroelect.* **36,** 3–20 (2001).
22. Stemmer, S., Streiffer, S. K., Ernst, F. & Rühle, M. Dislocations in $PbTiO_3$ thin films. *Phys. Stat. Sol. A* **147,** 135–154 (1995).
23. Watanabe, Y., Okano, M. & Masuda, A. Surface conduction on insulating $BaTiO_3$ crystal suggesting an intrinsic surface electron layer. *Phys. Rev. Lett.* **86,** 332–335 (2001).
24. Kakegawa, K., Mohri, J., Takahashi, T., Yamamura, H. & Shirasaki, S. A compositional fluctuation and properties of Pb(Zr,Ti)O_3. *Solid State Commun.* **24,** 769–772 (1977).
25. Hellwege, K.-H. (ed.). *Landolt-Börnstein: Numerical Data and Functional Relationships in Science and Technology* (Springer, Berlin), *Group III: Crystal and Solid State physics* **1,** 66 (1966); **3,** 427 (1969); **16,** 64 (1981).
26. Matthews, J. W. & Blakeslee, A. E. Defects in epitaxial multilayers: I. Misfit dislocations. *J. Cryst. Growth* **27,** 118–125 (1974).
27. Suzuki, T., Takeuchi, S. & Yoshinaga, H. *Dislocation Dynamics and Plasticity* (Springer, Berlin, 1991).
28. Hÿtch, M. J., Snoeck, E. & Kilaas, R. Quantitative measurement of displacement and strain fields from HREM micrographs. *Ultramicroscopy* **74,** 131–146 (1998).
29. Jia, C. L. *et al.* Lattice strain and lattice expansion of the $SrRuO_3$ layers in $SrRuO_3$/$PbZr_{0.52}Ti_{0.48}O_3$/$SrRuO_3$ multilayer thin films. *J. Appl. Phys.* **92,** 101–105 (2002).

Acknowledgements

Part of this work was supported by Volkswagen Stiftung in the project 'Nano-sized Ferroelectric Hybrids' under the contract No. 5/77737, and part by DFG via FOR 404.
Correspondence and requests for materials should be addressed to M.W.C.

Competing financial interests

The authors declare that they have no competing financial interests.